Available online at www.sciencedirect.com
ScienceDirect
Catalysis Today 136 (2008) 64–75
CATALYSIS TODAY
www.elsevier.com/locate/cattod

A DFT study of adsorption of intermediates in the NO_x reduction pathway over BaNaY zeolites

Chun-Yi Sung, Linda J. Broadbelt *, Randall Q. Snurr *

Institute for Catalysis in Energy Processes, Chemical and Biological Engineering Department, Northwestern University, 2145 Sheridan Road, Evanston, IL 60208, USA

Available online 7 March 2008

Abstract

Quantum chemical calculations were employed to develop a better understanding of the adsorption properties of BaNaY interacting with molecules relevant to deNO_x catalysis. First, various basis sets and levels of theory were tested for barium-containing species and gas-phase reactions, and it was shown that the choice of the basis set for barium is critical. Density functional theory (DFT) with the B3LYP functional and SDD as the basis set was selected based on its combination of relative accuracy and speed. This level of theory was then used to calculate energies, geometries, and frequencies for acetaldehyde, acetic acid, nitromethane, and water adsorbed and in the gas phase. The predicted properties were compared to experiment where available and reasonable agreement was found. To study the effect of the zeolite framework on the adsorption properties, the size of the zeolite cluster was increased from 6 T to 36 T to 96 T using the embedded ONIOM method. Inclusion of van der Waals interactions with increasing cluster size only changed the adsorption enthalpy by a small amount for all of the adsorbates studied. It was found that the interaction between the empty 6s orbital of Ba and the lone pair orbital of the oxygen atom in the adsorbed state, revealed by natural bond orbital analysis, correlates with the adsorption enthalpy and the gas-phase charge of the oxygen atom that interacts with Ba.

Keywords: deNO_x; ONIOM; Zeolites; Catalysis

1. Introduction

Nitrogen oxides (NO_x), including nitrogen dioxide (NO_2) and nitric oxide (NO), play an important role in the atmospheric reactions that create smog and acid rain, and therefore affect many ecosystems as well as human health. One of the major emission sources is transportation vehicles [1]. In the early 1980s emission standards for NO_x in the US were tightened to the point that a catalyst for converting NO_x was needed [2]. Since then numerous catalysts have been studied for NO_x reduction, such as CuZSM-5, CoZSM-5, CoFER, GaZSM-5, and PdZSM-5 [3–8], as well as other approaches such as NO_x trapping [9] or a combination of catalysis and a non-thermal plasma [10,11].

Recently, BaNaY zeolites have received attention since it has been reported that acetaldehyde, which is formed from hydrocarbons in a non-thermal plasma, reduces NO_x to N_2 over BaNaY catalysts at relatively low temperature [10]. A large increase in NO_x reduction activity was found with the introduction of Ba^{2+} ions into NaY zeolites [11]. Using FTIR spectroscopy and isotopic labeling, important insights have been obtained about the chemistry of the deNO_x reactions over BaNaY zeolites, and a detailed mechanism for the formation of N_2 from NO_2 and NO interacting with acetaldehyde or acetic acid has been proposed [12]. However, the role that Ba plays in the catalytic reduction reactions remains unclear. To shed further light on the catalytic nature of BaNaY zeolites, it is important to have a better understanding of the adsorption properties of key reaction intermediates on the barium cations. We therefore studied the adsorption of acetaldehyde, acetic acid, nitromethane, and water on BaY theoretically using density functional theory (DFT). In the deNO_x mechanism, acetaldehyde and acetic acid are reductants, nitromethane is thought to be a key intermediate, and water is evolved during several proposed dehydration steps.

For atoms in the lower part of the periodic table like barium, an effective core potential (ECP) is usually applied in quantum

* Corresponding authors.
E-mail addresses: broadbelt@northwestern.edu (L.J. Broadbelt), snurr@northwestern.edu (R.Q. Snurr).

0920-5861/$ – see front matter
doi:10.1016/j.cattod.2008.01.010

chemical studies. An ECP uses a potential to represent the large number of core electrons that are not directly involved in the chemistry. An ECP can also account for relativistic effects to some extent. We first examined different possible basis sets for barium by testing the performance of LANL2DZ [13] and WB MEFIT [14] ECPs for barium combined with various all-electron basis sets for the other atoms using DFT. To assess these methods, calculated geometric parameters of barium dihalides and heats of reaction for representative gas-phase reactions involving barium were compared to experimental values from the literature.

For zeolites that contain hundreds of atoms per unit cell, the use of periodic ab initio methods is too expensive, and therefore hybrid methods, such as the ONIOM method [15], are often used. In this study, we employed the two-layer ONIOM method, which treats the region of interest for adsorption using quantum mechanics and the surrounding zeolitic framework with a molecular mechanics force field. Van der Waals interactions are known to be important in zeolites [16–18], but DFT does not generally represent van der Waals interactions well. An attractive feature of QM/MM methods such as ONIOM is that force fields explicitly include these weak van der Waals interactions. We therefore tested the effect of van der Waals interactions on the geometry, vibrational frequencies, and energetics of the adsorbates by using different sizes of clusters.

2. Computational methods

2.1. Basis set study

Two ECP basis sets were explored for barium, namely LANL2DZ [13] and the multi-electron adjusted quasirelativistic effective core potential (WB-MEFIT). The WB-MEFIT ECP was used along with the 6s6p5d1f valence basis set (denoted as SDD in the text) developed by Kaupp et al. [14]. The 6s6p5d1f valence basis set of SDD was contracted in two ways: 3111/3111/32/1 and 3111/3111/311/1. For carbon, oxygen, hydrogen and halogen atoms, two types of all-electron basis sets were used: Dunning/Huzinaga double zeta basis sets, D95 or D95(d,p), and the Pople basis set 6-311++G(d,p). Two different DFT functionals were tested: PW91PW91 [19] and B3LYP [20]. All calculations were carried out using Gaussian 03 [21].

2.2. Cluster model

Yeom et al. reported that in zeolite X, Ba^{2+} ions are found at sites I, I′, and II by single-crystal X-ray diffraction techniques, and the majority of them are located at site II [22]. These sites are depicted in Fig. 1. A few years later, Martra et al. also found that in BaY zeolite, Ba^{2+} ions substitute almost completely for the Na^{+} ions at site II, as revealed by IR spectroscopy of adsorbed CO and CO_2[23]. Therefore, site II was considered as the active site in this study.

Y zeolites have unit cells of 576 atoms, which are too large for an entire unit cell to be considered in quantum chemical calculations. Therefore, zeolite cluster models were utilized. A portion of the zeolite including a single six ring (S6R) next to

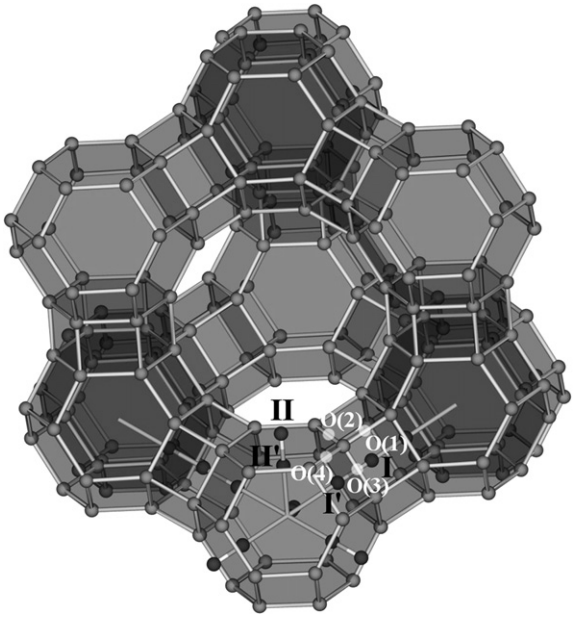

Fig. 1. Structure of faujasite zeolite showing sites I, I′, II, and II′ where Ba^{2+} ions are labeled. The majority of them are located at site II.

site II was extracted from the crystal structure of Y zeolite taken from the results of high-resolution time-of-flight neutron powder diffraction reported by Hriljac et al. [24]. The terminating Si and O atoms were fixed at their crystallographic positions and saturated with hydrogen atoms directed along the bond vector of what would have been the next zeolite framework atom in the crystal structure. The Si–H and O–H distances were fixed at 1.49 and 0.96 Å, respectively. The terminating SiH_3 or OH groups were held fixed in all geometry optimizations, and all other atomic positions were optimized to find the lowest energy. Many researchers have used similar quantum chemical methodologies to investigate metal-exchanged zeolites [25–29].

Two aluminum atoms are required for the cluster to be charge neutral when one Ba atom is included in the zeolite cluster. The location of the aluminum atoms is limited by Löwenstein's rule, which states that two aluminum-centered tetrahedra cannot share an oxygen atom. Due to the symmetry of the S6R, there are only two possible aluminum arrangements, and they were denoted here as 1,3 and 1,4, respectively, with the numbering based on the relative positions of the aluminum atoms in the ring. Two different cluster sizes were chosen: one with 6 T atoms denoted as cluster A and the other one with 10 T atoms, which included the 6 T atoms in the ring and additional SiH_3 groups around the two Al atoms, denoted as cluster B. Given the possibilities for the aluminum atom arrangements and the two different cluster sizes, there were four different cluster geometries: A-1,3, A-1,4, B-1,3, and B-1,4, as shown in Fig. 2. These clusters will be referred to as quantum clusters, since they were calculated with only quantum mechanics.

To incorporate the effects of the surrounding zeolite framework, the QM/MM method ONIOM [15] was used with a cluster model that consisted of two layers linked via

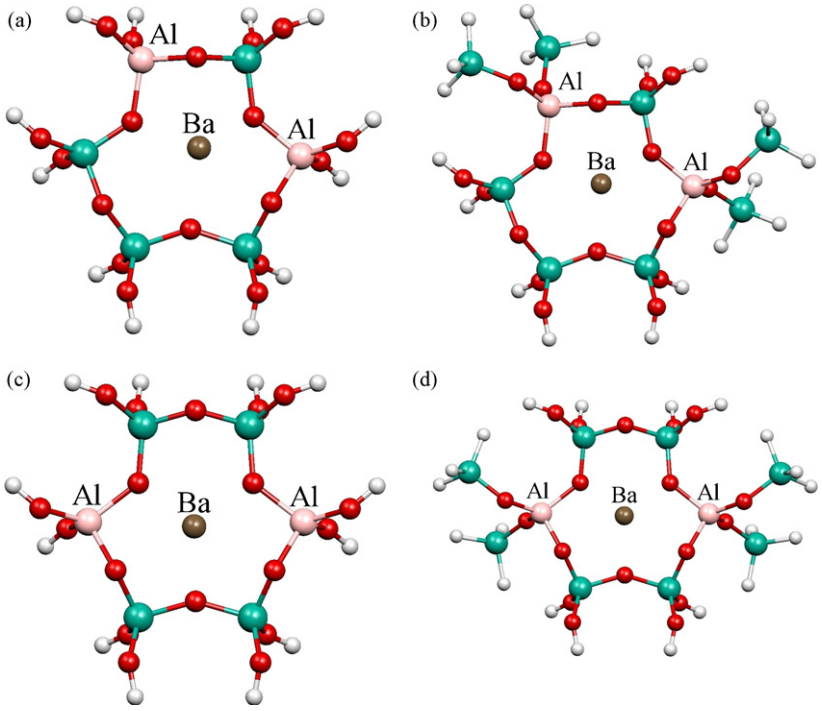

Fig. 2. Structure of BaY around site II:(a) A-1,3, (b) B-1,3, (c) A-1,4 and (d) B-1,4. The clusters denoted as A have 6 T atoms, while the clusters denoted as B have 10 T atoms. The 1,3 and 1,4 notations denote the relative positions of the two aluminum atoms in the S6R. Hydrogen atoms are shown in light gray, oxygen atoms are shown in red, aluminum atoms are shown in pink, silicon atoms are shown in green, and Ba is shown in brown.(For interpretation of the references to colour in this figure legend, the reader is referred to the web version of the article.)

mechanical embedding. The inner layer consisted of the 6 T atoms that are the same as those modeled in the quantum clusters. An inner layer of 10 T atoms was not used based on the results of the four different clusters in Fig. 2, as discussed in Section 3.2.1. The outer layer consisted of 30 or 90 T atoms that were located symmetrically around the inner 6 T atoms. Thus, in total, the ONIOM clusters consisted of 36 or 96 T atoms, as shown in Fig. 3. These two sizes of ONIOM clusters allowed us to assess the sensitivity of the calculated properties to long-range van der Waals interactions and the ability of the different cluster sizes to include these interactions. All atoms in the S6R, barium and atoms comprising the adsorbates were allowed to relax. All other atoms were fixed at their crystallographic positions.

The total energy of the whole system studied with the two-layer ONIOM approach is expressed as:

$$E_{\mathrm{ONIOM}} = E_{\mathrm{High}}^{\mathrm{Cluster}} + E_{\mathrm{Low}}^{\mathrm{System}} - E_{\mathrm{Low}}^{\mathrm{Cluster}} \quad (1)$$

where the superscript ‘‘Cluster’’ denotes the inner layer, and the superscript ‘‘System’’ designates the whole zeolitic framework utilized. Subscripts ‘‘High’’ and ‘‘Low’’ denote energies obtained at the high and low levels of theory, respectively. In this study, the quantum cluster models were treated using density functional theory, which also served as the high level of theory in the ONIOM calculations. The low level of theory in the ONIOM calculations was molecular mechanics using the universal force field (UFF) [30]. The UFF atom types for Si, O, and Al were specified as Si3, O_3_z, and Al3, respectively.

Infrared frequencies were calculated for each adsorbate studied. Many vibrational modes calculated by Gaussian 03 were originally imaginary due to the artificial condition that the terminal groups of the clusters were fixed, and many nonimaginary modes were spurious because of the coupling between the terminal groups and the rest of the cluster. These vibrational modes were removed by the level-shift technique [25,31]. The level-shifted frequencies were then used to calculate the adsorption enthalpy and the change of Gibbs free energy upon adsorption within the rigid rotor, harmonic oscillator approximation. No scale factor was available for the particular combinations of functional and basis set that we employed, so the frequencies were used unscaled. In order to obtain more reliable interaction energies, basis set superposition error (BSSE) corrections using the counterpoise method [32] were taken into account. The calculated values were compared to experiments where available. The energetic stabilization due to donor–acceptor interactions between barium and the adsorbates and the associated charge transfer were quantified using natural bond orbital analysis (NBO) [33,34]. The interactions of adsorbates with a bare Ba^{2+} ion were also calculated for comparison.

3. Results and discussion

3.1. Basis set study

3.1.1. Apex angles of barium dihalides

The calculated apex angles of BaF_2, $BaCl_2$, and $BaBr_2$ using different basis set combinations are listed in Table 1 and compared with experimental values [35–38]. In addition, calculations in the literature using different methods are

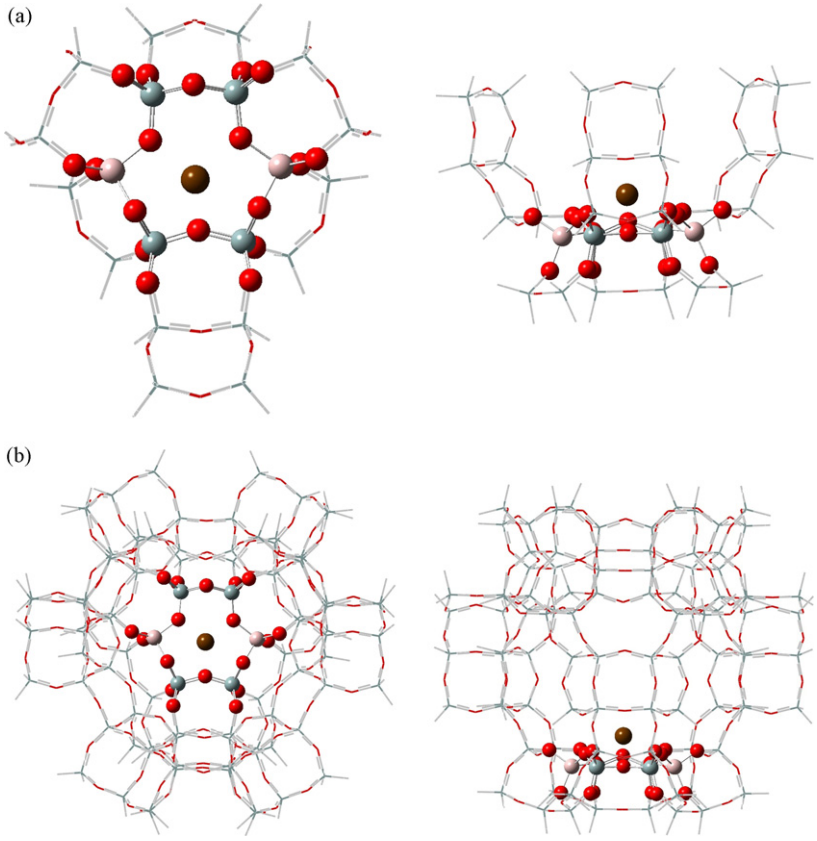

Fig. 3. Structures of the (a) 36 T and (b) 96 T clusters used for ONIOM calculations. Atoms treated with DFT are shown in a ball and stick representation, and atoms treated with molecular mechanics are shown in a wireframe representation. Oxygen atoms are shown in red, aluminum atoms are shown in pink, silicon atoms are shown in green, and Ba is shown in brown.The left hand side presents a top view, and the right hand side offers a side view. (For interpretation of the references to colour in this figure legend, the reader is referred to the web version of the article.)

summarized. Results for some combinations were obtained with only SDD or LANL2DZ ECP basis sets for both barium and bromine because D95 and D95(d,p) basis functions are not available for bromine.

For the three barium dihalides studied, a linear or close-to-linear (165–180°) structure was calculated when LANL2DZ was utilized for barium. All other calculations indicate that the three barium dihalides are bent, in agreement with experiments. For various SDD/all-electron combinations of basis sets, the differences between the angles calculated using B3LYP and PW91PW91 are within 3° for BaF_2 and $BaCl_2$ and within 6° for $BaBr_2$.

3.1.2. Heats of reaction of barium-containing reactions

Heats of reaction for four different reactions involving barium compounds were calculated at 298.15 K in the gas phase.

$$Ba + H_2O \rightarrow BaOH + H \quad (I)$$

$$Ba + 2H_2O \rightarrow Ba(OH)_2 + 2H \quad (II)$$

$$Ba + CO_2 \rightarrow BaO + CO \quad (III)$$

$$Ba + N_2O \rightarrow BaO + N_2 \quad (IV)$$

The combinations of basis sets used above were used again with the B3LYP and PW91PW91 functionals. Enthalpies were calculated as follows:

$$H = E_0 + E_{ZPE} + E_v + E_t + E_r + RT \quad (2)$$

where E_0 is the electronic energy, E_{ZPE} is the zero-point energy, E_v is the internal energy due to vibration, E_t is the internal energy due to translation, and E_r is internal energy due to rotation. The calculated values are compared with experimental heats of reaction [39] as summarized in Table 2. The mean absolute deviation for each basis set and method combination based on all four reactions is reported in Table 3.

For the four gas phase reactions studied, LANL2DZ predicts the heat of reaction poorly for both B3LYP and PW91PW91. For reaction (I), B3LYP gives slightly better results than PW91PW91. For SDD, the method that gave the best agreement with the experimental values depended on the reaction studied. Among the B3LYP calculations, the SDD basis set contracted in 3111/3111/311/1 for barium with 6-311++G(d,p) for oxygen and hydrogen atoms predicted the heats of reaction the best compared to the experimental values for reactions (I) and (II). For reaction (II), only B3LYP calculations were carried out since it resembles reaction (I). For reaction (III), the heat of reaction calculated with the SDD/D95

Table 1
Apex angles of barium dihalides calculated using different functional and basis set combinations and obtained from experiments

Basis set		Method						Ref.
Ba	Halide	BaF_2		$BaCl_2$		$BaBr_2$		
		B3LYP	PW91PW91	B3LYP	PW91PW91	B3LYP	PW91PW91	
LANL2DZ	D95	180	180	171	169	180 [a]	180 [a]	
LANL2DZ	D95(d,p)	180	180	170	165	180 [a]	180 [a]	
LANL2DZ	6-311++G(d,p)	175	168	166	165	180	180	
SDD [b]	D95	119	117	130	127	133 [a]	127 [a]	
SDD [b]	D95(d,p)	118	115	128	126	133 [a]	127 [a]	This work
SDD [b]	6-311++G(d,p)	123	121	129	127	133	128	
SDD [c]	D95	119	117	129	127	132 [a]	127 [a]	
SDD [c]	D95(d,p)	117	115	128	126	132 [a]	127 [a]	
SDD [c]	6-311++G(d,p)	123	121	129	126	131	126	
SDD [d]	cc-pVTZ	118		128				[42]

Basis set		HF			Ref.
SDD [e]	pp [f]	125	145	153	[43]
SDD [g]	pp [f]	126	142	147	[43]

Basis set		SDCI+Q			Ref.
SDD [d]	pp [h]	123	141	143	[43]
Experiment		100	100 120	137	[35–38]

[a] Both barium and halogen atoms were calculated with SDD or LANL2DZ ECP basis sets.
[b] WB-MEFIT ECP and 6s6p5d1f basis set with contraction pattern 3111/3111/32/1.
[c] WB-MEFIT ECP and 6s6p5d1f basis set with contraction pattern 3111/3111/311/1.
[d] WB-MEFIT ECP and 6s6p5d1f basis set with contraction pattern 111111/111111/11111/1.
[e] WB-MEFIT ECP and 6s6p5d basis set with contraction pattern 111111/111111/32.
[f] pp: pseudopotential with valence basis set with contraction pattern 311/311/1.
[g] WB-MEFIT ECP and 6s6p5d basis set with contraction pattern 111111/111111/11111.
[h] pp: pseudopotential with valence basis set with contraction pattern 2111/2111/1.

basis set using B3LYP agrees the best with the experimental value, and this combination predicted the heat of reaction of reaction (IV) well also. Overall, the mean absolute deviations tabulated in Table 3 identify B3LYP/SDD/6-311++G(d,p) as the level of theory that captures the heats of reaction of reactions involving barium the best.

3.1.3. Selection of basis set for cluster calculations

Combining all of these results together led to the selection of the SDD basis set with its 6s6p5d1f valence basis set contracted in the form of 3111/3111/32/1 for barium and D95 for other atoms in our cluster calculations (Si, Al, O, C, N, and H) to perform the adsorption studies. This combination is the

Table 2
Heats of reaction involving barium calculated using different functional and basis set combinations and compared to experimental values

Basis set		Method						
Ba	X [a]	I		II	III		IV	
		B3LYP	PW91PW91	B3LYP	B3LYP	PW91PW91	B3LYP	PW91PW91
LANL2DZ	D95	39.4	37.4	63.7	67.7	78.8	−13.1	2.61
LANL2DZ	D95(d,p)	52.4	50.1	89.6	83.8	92.7	−0.22	14.4
LANL2DZ	6-311++G(d,p)	38.6	35.7	61.6	71.7	79.3	−15.1	−2.01
SDD [b]	D95	1.47	−4.53	6.48	−5.69	−7.01	−86.5	−83.2
SDD [b]	D95(d,p)	14.5	8.33	36.1	9.28	6.29	−74.8	−72.0
SDD [b]	6-311++G(d,p)	14.3	8.27	28.9	9.97	6.39	−76.8	−74.9
SDD [c]	D95	0.42	−5.73	5.57	−6.83	−8.26	−87.62	−84.7
SDD [c]	D95(d,p)	13.3	6.90	30.4	7.15	3.98	−76.9	−74.3
SDD [c]	6-311++G(d,p)	13.1	6.92	27.6	7.92	4.28	−78.8	−77.0
Experiment[39]		12.9		27.2	−4.77		−92.0	

Values are reported in kcal/mol.
[a] X denotes C, N, O or H.
[b] WB-MEFIT ECP and 6s6p5d1f basis set with contraction pattern 3111/3111/32/1.
[c] WB-MEFIT ECP and 6s6p5d1f basis set with contraction pattern 3111/3111/311/1.

Table 3
Mean absolute deviation [a] between the calculated values of the heats of reaction and the experimental values based on all four reactions

Basis set		Method	
Ba	X [b]	B3LYP	PW91PW91
LANL2DZ	D95	53.6	67.6
LANL2DZ	D95(d,p)	70.6	80.3
LANL2DZ	6-311++G(d,p)	53.4	65.6
SDD [c]	D95	9.65	9.50
SDD [c]	D95(d,p)	10.4	11.9
SDD [c]	6-311++G(d,p)	8.25	11.0
SDD [d]	D95	10.1	9.90
SDD [d]	D95(d,p)	7.65	10.8
SDD [d]	6-311++G(d,p)	6.63	10.0

Values are reported in kcal/mol.
[a] Mean absolute deviation defined as $\sum_i^N |\Delta H_{ri,QC} - \Delta H_{ri,\exp}|/N$ where QC denotes the quantum chemical value, exp denotes the experimental value, and N is equal to 4 for B3LYP and 3 for PW91PW91.
[b] X denotes C, N, O or H.
[c] WB-MEFIT ECP and 6s6p5d1f basis set with contraction pattern 3111/3111/32/1.
[d] WB-MEFIT ECP and 6s6p5d1f basis set with contraction pattern 3111/3111/311/1.

smallest one among the series of SDD/all-electron basis sets studied, yet its mean absolute deviation is only 3 kcal/mol higher than the most accurate and most expensive one. The B3LYP and PW91PW91 functionals gave similar results for most properties. B3LYP was chosen as the functional for the studies of the quantum clusters and the high-level of theory in ONIOM based on its widespread use in literature. LANL2DZ using either B3LYP or PW91PW91 was ruled out because its predictions of the apex angle of barium dihalides and the heats of reaction of gas phase reactions involving barium compounds were not reasonable.

3.2. BaY cluster models

3.2.1. Pure quantum cluster models

Four different cluster models were considered as shown in Fig. 2. The electronic properties, i.e., the charge and electronic configuration of Ba will likely influence the adsorption properties of different adsorbates strongly, so the first analysis was aimed at uncovering how cluster size and aluminum arrangement affected the electronic properties. The NBO charge on Ba and its electronic configuration are shown for the four different clusters in Table 4. The charge and electronic configurations of Ba are almost independent of the Al atom arrangements and the size of the cluster models considered. To reduce computational cost, we therefore only employed the A cluster (6 T) as the pure quantum cluster model and as the inner layer of the ONIOM model, and only the 1,4 aluminum arrangement was used in subsequent calculations.

Table 4
Natural bond orbital charges and electronic configurations of Ba in different BaY cluster models defined in Fig. 2 calculated using B3LYP/SDD/D95

Cluster	NBO charge of Ba	Electronic configuration of Ba
A-1,3	1.910	Core[53.97]6s[0.05]5d[0.06]6p[0.01]
A-1,4	1.915	Core[53.97]6s[0.05]5d[0.05]6p[0.01]
B-1,3	1.921	Core[53.96]6s[0.05]5d[0.05]6p[0.01]
B-1,4	1.917	Core[53.96]6s[0.05]5d[0.05]6p[0.01]

3.2.2. Displacement of cation from six-ring plane

There are four types of oxygen atoms in faujasite zeolites: O(1), O(2), O(3), and O(4) as shown in Fig. 1. In the BaX structure reported by Yeom et al. [22], the Ba atoms that lie at site II are extended 1.12 Å into the supercage from the plane formed by three O(2) atoms in the S6R. In our cluster calculations, the Ba atom at site II is 1.639 Å above the O(2) plane in the 6 T cluster, and it only decreases slightly to 1.637 Å when the cluster size increases up to 96 T. It should be noted that in Y zeolites, the cation concentration is lower than in X zeolites. Therefore, the Ba atom should be less strongly anchored inside the zeolitic framework in zeolite Y to compensate for the electric charges of the aluminum atoms [40]. This is consistent with the calculated position being more extended toward the supercage by 0.5 Å than in the reported BaX structure.

3.3. Adsorption of water, acetaldehyde, nitromethane, and acetic acid

3.3.1. Structures

Several different initial configurations were explored for each of the adsorbates, and the optimized geometries that were the most stable are shown in Fig. 4. Selected geometric parameters are shown in Table 5. All the adsorbates studied are adsorbed through an interaction between Ba and an adsorbate oxygen atom, with a distance of 2.62–2.81 Å. This distance is 0.2–0.3 Å longer than when the molecules interact with a bare Ba^{2+} ion. The α bonds of the oxygen atom interacting with Ba, such as C=O in acetaldehyde and acetic acid or N–O in nitromethane, are elongated from their values in the gas phase on both the clusters and bare Ba^{2+}. On the other hand, the bonds β from Ba, C–C in acetaldehyde, N–O in nitromethane and C–O in acetic acid, are shortened on the clusters compared to their gas-phase values, with the values in the bare Ba^{2+} case as the lower limit.

It is interesting that in the most stable structures found for acetaldehyde and nitromethane, one of the hydrogen atoms in the methyl group is coordinated to a framework oxygen next to an aluminum atom at a distance of 1.94–2.02 Å for nitromethane and 2.03–2.36 Å for acetaldehyde, with the longest value corresponding to the largest cluster (96 T). In contrast, the hydrogen atom of the hydroxyl group in acetic acid is coordinated to the same framework oxygen with a much shorter distance of 1.37–1.45 Å. Furthermore, the more positive the hydrogen is, the more the system can be stabilized by its coordination to the framework oxygen. DFT calculations of gas phase acetic acid give a charge of +0.49 on the hydroxyl hydrogen and +0.14–0.16 on the methyl hydrogens. Adsorbed acetic acid is thus more stabilized by a geometry where the hydroxyl hydrogen can interact with a zeolitic oxygen atom. Similarly, adsorbed acetaldehyde is more stabilized with a

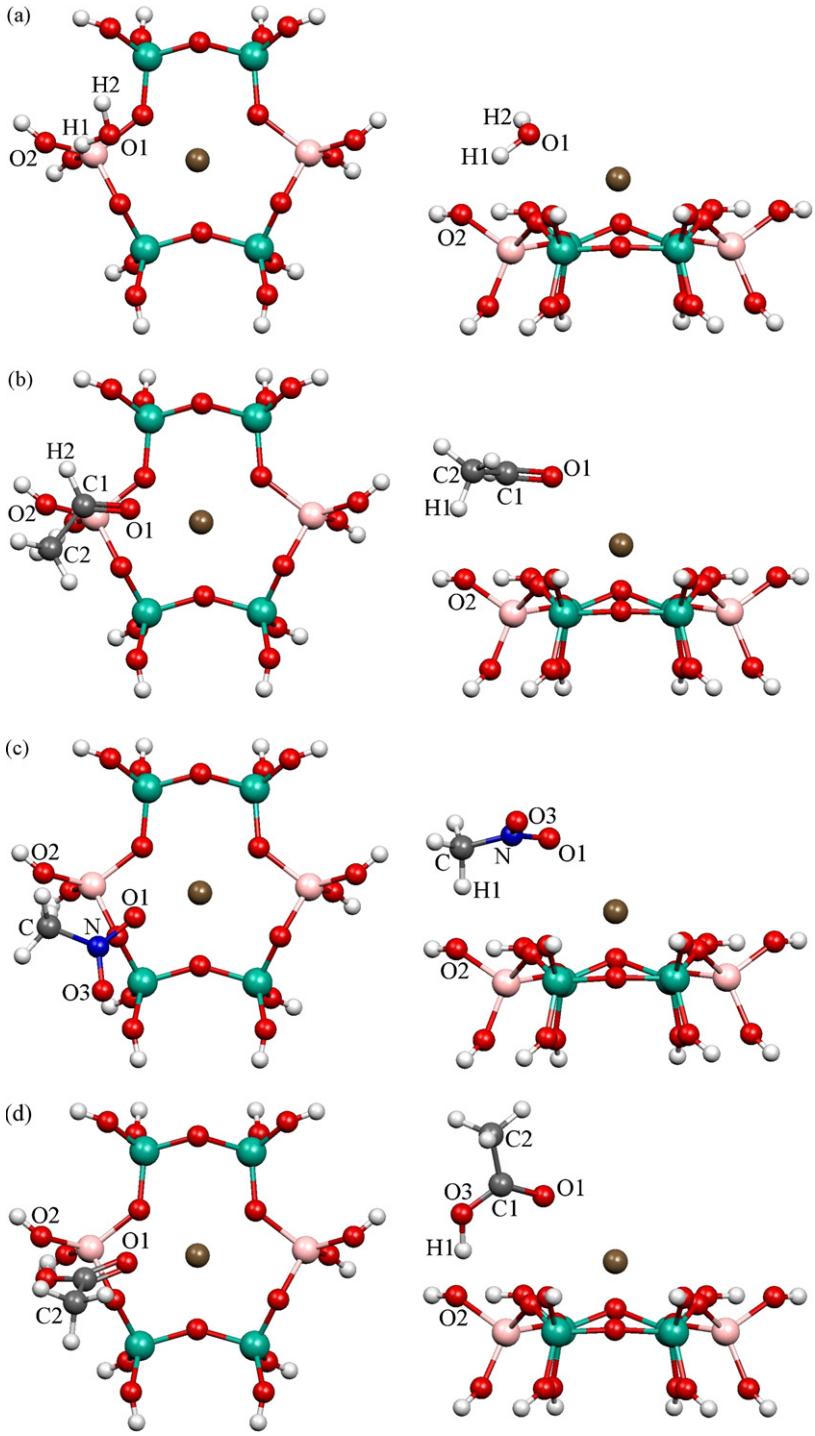

Fig. 4. Structure of adsorbed (a) H_2O, (b) acetaldehyde, (c) nitromethane, and (d) acetic acid on 96 T BaY clusters. Only the QM portions are shown for simplicity. Hydrogen atoms are shown in light gray, oxygen atoms are shown in red, carbon atoms are shown in dark gray, nitrogen atoms are shown in blue, aluminum atoms are shown in pink, silicon atoms are shown in green, and Ba is shown in brown. The left hand side presents a top view, and the right hand side offers a side view. (For interpretation of the references to colour in this figure legend, the reader is referred to the web version of the article.)

methyl hydrogen atom, that has a gas-phase charge of +0.09–0.12, oriented toward the framework oxygen instead of the aldehyde hydrogen atom with a gas-phase charge of −0.03.

It is clear from Table 5 that the cluster size has very little influence on the geometric parameters. This reveals that the configurations of the adsorbates on the 6T cluster would not be hindered spatially by the zeolite framework outside of the 6 T cluster. The supercage above the S6R is sufficiently large to accommodate the small adsorbates studied here.

3.3.2. *Frequencies*

The characteristic frequencies of acetaldehyde, nitromethane, and acetic acid both in the gas phase and adsorbed on the A-1,4 clusters are listed and compared with experimental

Table 5
Selected geometric parameters of gas-phase and adsorbed H_2O, acetaldehyde, nitromethane, and acetic acid on a Ba^{2+} ion and 1,4 aluminum BaY clusters of different sizes

	Distance (Å)				Angle (°)
	O1–H2	O1–H1	Ba–O1	H1–O2	H1–O1–H2
H_2O					
Gas phase	0.98	0.98			110
Ba^{2+}	0.99	0.99	2.56		107
BaY(6 T)	0.98	1.01	2.81	1.88	109
BaY(36 T)	0.98	1.00	2.79	1.91	109
BaY(96 T)	0.98	1.00	2.80	1.91	109

	Distance (Å)					Angle (°)	
	C1–H2	C1–O1	C1–C2	Ba–O1	H1–O2	O1–C1–H2	Ba–O1–C1
Acetaldehyde							
Gas phase	1.11	1.24	1.51			120	
Ba^{2+}	1.10	1.28	1.47	2.41		117	177
BaY(6 T)	1.11	1.26	1.49	2.71	2.03	118	142
BaY(36 T)	1.11	1.26	1.49	2.69	2.34	119	140
BaY(96 T)	1.10	1.26	1.49	2.69	2.36	119	140

	Distance (Å)					Angle (°)	
	N–O1	N–O3	N–C	Ba–O1	H1–O2	O1–N–O3	Ba–O1–N
Nitromethane							
Gas phase(e [a])	1.28	1.27	1.51			125	
Gas phase(s [a])	1.27	1.27	1.51			125	
Ba^{2+}	1.33	1.24	1.51	2.43		121	160
BaY(6 T)	1.29	1.26	1.50	2.74	1.94	123	133
BaY(36 T)	1.29	1.26	1.50	2.74	2.01	123	135
BaY(96 T)	1.29	1.26	1.50	2.74	2.02	123	135

	Distance (Å)						Angle (°)	
	C1–O1	C1–O3	C1–C2	H1–O3	Ba–O1	H1–O2	O1–C1–O3	Ba–O1–C1
Acetic acid								
Gas phase	1.24	1.39	1.51	0.98			122	
Ba^{2+}	1.30	1.32	1.49	0.99	2.39		121	172
BaY(6 T)	1.27	1.32	1.51	1.10	2.62	1.37	124	153
BaY(36 T)	1.27	1.32	1.51	1.07	2.63	1.45	125	150
BaY(96 T)	1.27	1.32	1.51	1.07	2.63	1.45	124	149

The atom labels are defined in Fig. 4
[a] The e designation refers to eclipsed, while the s designation refers to staggered.

values where available in Table 6. When a direct experimental comparison is possible, it is observed that the calculated frequencies have relative errors within 5%. For the C = O stretching frequency of adsorbed acetic acid, there is no definite frequency assigned to this mode based on experimental data of adsorbed acetic acid on BaNaY zeolite [12]. However, a close correspondence can be found in the spectrum of acetic acid on MgO, where 1570 cm^{-1} was assigned to C = O stretching of a monolayer of adsorbed acetic acid on MgO [41]. Note that the data in Table 6 show that increasing the size of the cluster did not affect the prediction of the characteristic frequencies of these adsorbates markedly. The calculated frequencies here are mostly underestimated compared to experimental values.

Table 6
Characteristic frequencies of gas phase and adsorbed acetaldehyde, nitromethane, and acetic acid compared to experimental values from the literature

	Acetaldehyde	Nitromethane	Acetic acid
Characteristic frequency	C = O stretch	NO_2 stretch	C = O stretch
Gas phase	1709	1515	1728
Experiment (gas phase)	1774[44]	1583[45]	1788[46]
Ba^{2+}	1603	1546	1538
BaY (6 T)	1655	1534	1575
BaY (36 T)	1669	1529	1590
BaY (96 T)	1669	1529	1593
Experiment (adsorbed)	1704[12]	1556[12]	1570[41]

All frequencies are reported in cm^{-1}.

3.3.3. Changes in enthalpy and Gibbs free energy upon adsorption

To calculate the adsorption enthalpy and the change of Gibbs free energy upon adsorption, three energies were calculated. The energy of the bare zeolite cluster and the energy of the zeolite cluster interacting with the adsorbate were both calculated by the two-layer ONIOM approach as in Eq. (1), and the energy of the adsorbate in the gas phase was calculated

purely by DFT. With corrections included to all three quantities as summarized in Eq. (2), enthalpies were obtained, and they are denoted as H^{Z}_{ONIOM}, H^{Z+X}_{ONIOM}, and H^{X}_{DFT}, respectively. Then the adsorption enthalpy was calculated by:

$$\Delta H = H^{Z+X}_{ONIOM} - H^{Z}_{ONIOM} - H^{X}_{DFT} \quad (3)$$

In both H^{Z}_{ONIOM} and H^{Z+X}_{ONIOM}, there is a contribution from the inner layer calculated at the high level of theory, i.e., DFT, which is the first term in the right hand side of Eq. (1). If the contributions from the inner layer calculated with DFT from both H^{Z}_{ONIOM} and H^{Z+X}_{ONIOM} are collected together with H^{X}_{DFT}, ΔH can be deconvoluted into two parts: the adsorption enthalpy from quantum mechanics, ΔH_{QM}, and the adsorption enthalpy from molecular mechanics, ΔH_{MM}:

$$\Delta H = \Delta H_{QM} + \Delta H_{MM} \quad (4)$$

The adsorption enthalpies of water, acetaldehyde, nitromethane, and acetic acid on the 6 T, 36 T, and 96 T clusters are listed in Table 7 at 298.15 K. ΔH is also decomposed into its contributions from the QM and MM parts as in Eq. (4). For all the adsorbates studied, it can be seen that as the size of the cluster increases, the contribution to the adsorption enthalpy from the QM part is relatively invariant, whereas the contribution from the MM part increases non-linearly, suggesting that an asymptotic value of ΔH_{MM}, and thus ΔH, is being approached. Considering that the configurations of the adsorbates barely change on clusters of different sizes, it can be understood that the changes in the adsorption enthalpies are due to the inclusion of the increasing van der Waals interactions when the size of the outer layer of the cluster is increased. Unfortunately, only limited experimental data are available to compare to the predicted adsorption enthalpies. The experimental value of 28.7 kcal/mol [40] for adsorption of water on BaY agrees reasonably well with the value of 24.3 kcal/mol obtained for the 96 T cluster. Note that increasing the cluster size brought the predicted and experimental values in better agreement.

The change of Gibbs free energies upon adsorption for water, acetaldehyde, nitromethane, and acetic acid on the 6 T, 36 T, and 96 T clusters are also listed in Table 7 at 298.15 K, and the working temperature of the experiments of Yeom et al. [12](473 K). At 298.15 K, the change in Gibbs free energies upon adsorption for all adsorbates studied decreases as the cluster size increases from 6 T to 96 T, and they are all negative, meaning that adsorption is favored at 298.15 K. However, the Gibbs free energies upon adsorption increase markedly at 473 K from the values at 298.15 K. For nitromethane, only the change of the Gibbs free energy upon adsorption on the 96 T cluster is negative. Since adsorbed nitromethane on BaNaY was observed at 473 K in the experiments [12], these results suggest that a cluster size of at least 96 T is necessary for predicting adsorption of this species correctly.

3.4. Charge transfer and orbital interactions from NBO analysis

Natural bond orbital analysis is a technique that can transform ab initio wave functions into natural bond orbitals (NBOs) that describe molecular structures in terms of Lewis-like structures of electron pairs, such as core orbitals, lone pairs, and σ and π bonds. The general transformation to NBOs also leads to orbitals with small occupancies that correspond to unoccupied orbitals in the Lewis-like structural pictures, such as valence antibonding orbitals. These non-Lewis-type NBOs provide a correction (energy lowering) to the total energy that is dominated by the contributions from Lewis-type NBOs. The energy lowering, $\Delta E^{(2)}_{i \rightarrow j*}$, resulting from the interaction between a doubly occupied "donor" orbital ϕ_i and an

Table 7
Adsorption enthalpy at 298.15 K and free energy of adsorption at 298.15 K and 473 K for H_2O, acetaldehyde, nitromethane, and acetic acid as a function of cluster size

	ΔH (kcal/mol) at 298.15 K			ΔG (kcal/mol) at 298.15 K	ΔG (kcal/mol) at 473 K
	QM	MM	Total		
H_2O					
6 T	−22.6	0	−22.6	−12.3	−6.33
36 T	−22.6	−1.35	−24.0	−13.8	−7.86
96 T	−22.6	−1.64	−24.2	−14.1	−8.15
Acetaldehyde					
6 T	−18.6	0	−18.6	−6.0	1.24
36 T	−17.7	−4.06	−21.8	−10.8	−4.52
96 T	−17.8	−5.27	−23.1	−11.6	−5.06
Nitromethane					
6 T	−18.2	0	−18.2	−4.31	3.70
36 T	−18.2	−3.09	−21.3	−7.40	0.58
96 T	−18.1	−4.22	−22.3	−8.45	−0.46
Acetic acid					
6 T	−35.2	0	−35.2	−21.9	−14.1
36 T	−33.4	−2.29	−35.7	−21.9	−13.9
96 T	−33.6	−3.86	−37.5	−24.1	−16.4

The contributions to the adsorption enthalpy from quantum mechanics and molecular mechanics are reported separately.

unoccupied "acceptor" orbital ϕ_{j*} can be estimated by second-order perturbation theory [33,34]:

$$\Delta E^{(2)}_{i\rightarrow j*} = -2\frac{\langle\phi_i|\hat{F}|\phi_{j*}\rangle^2}{\epsilon_{\phi_{j*}} - \epsilon_{\phi_i}} \quad (5)$$

where $\hat{F}$ is the Fock operator, and ϵ_{ϕ_i} and $\epsilon_{\phi_{j*}}$ are the energies of the donor and acceptor orbitals. This energy lowering is also referred to as "donor–acceptor stabilization". The charge transferred from ϕ_i (donor) to ϕ_{j*} (acceptor), q, can be approximated as:

$$q \cong \frac{|\Delta E^{(2)}_{i\rightarrow j*}|}{\epsilon_{\phi_{j*}} - \epsilon_{\phi_i}} \quad (6)$$

Based on NBO analysis, it was found that the most significant donor–acceptor stabilization between Ba and the adsorbate molecules comes from the interaction between a valence lone pair orbital of the oxygen atom of the adsorbed molecule that is oriented towards Ba (shown in Fig. 5) and an unoccupied valence nonbonding orbital of Ba, which is mainly composed of the 6s orbital. Table 8 shows the stabilization energies and the amount of charge transfer associated with this interaction for adsorbed acetaldehyde, nitromethane, and acetic acid. The distance between Ba and the oxygen atom pointing toward Ba, the adsorption enthalpy, and the NBO charges of the same oxygen atom in the gas-phase molecule are also listed in Table 8. It can be seen that these properties exhibit the same trends among the three molecules. That is, as the value of $\Delta E^{(2)}_{i\rightarrow j*}$ increases (nitromethane, acetaldehyde and acetic acid), a greater amount of charge is transferred, and the Ba–O bond length decreases, as would be expected. This trend is also manifested in the overall adsorption enthalpies reported in Table 8. More interesting, however, is the simple correlation that exists between the NBO charge on the oxygen atom in the gas phase molecule and the adsorption enthalpies and the other properties in Table 8. The molecule with the most negative charge on oxygen in the gas phase adsorbs the most strongly, suggesting that the gas-phase

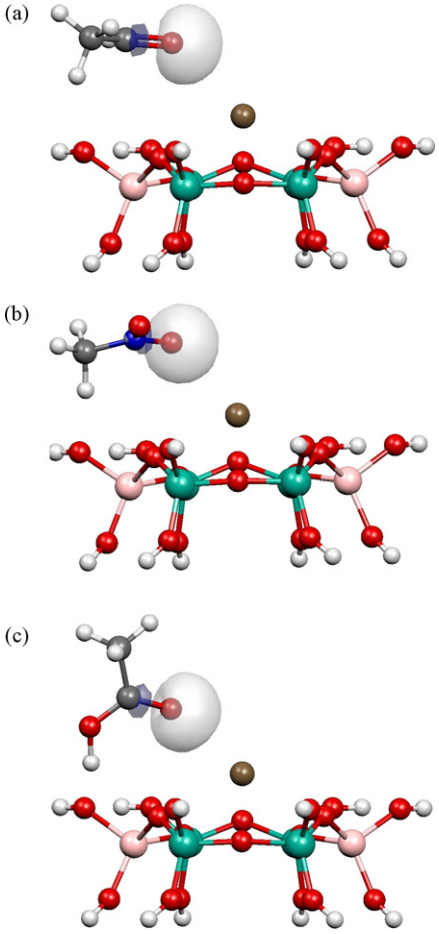

Fig. 5. The valence lone pair (donor) orbitals of oxygen in (a) acetaldehyde, (b) nitromethane, and (c) acetic acid are directed toward barium and are associated with donor–acceptor stabilization. Hydrogen atoms are shown in light gray, oxygen atoms are shown in red, carbon atoms are shown in dark gray, nitrogen atoms are shown in blue, aluminum atoms are shown in pink, silicon atoms are shown in green, and Ba is shown in brown. (For interpretation of the references to colour in this figure legend, the reader is referred to the web version of the article.)

Table 8
Donor–acceptor stabilization energy, $\Delta E^{(2)}_{i\rightarrow j*}$, and charge transferred, based on NBO analysis for adsorbed acetaldehyde, nitromethane, and acetic acid

	$\Delta E^{(2)}_{i\rightarrow j*}$ (kcal/mol)	Charge transferred (e)	Ba–O (Å)	ΔH (kcal/mol)	NBO charge of O of the adsorbates in gas phase
Acetaldehyde					
6 T	3.47	8.01×10^{-3}	2.71	−18.6	
36 T	3.45	8.27×10^{-3}	2.69	−21.8	−0.542
96 T	3.45	8.27×10^{-3}	2.69	−23.1	
Nitromethane					
6 T	3.37	7.21×10^{-3}	2.74	−18.2	
36 T	3.42	7.37×10^{-3}	2.74	−21.3	−0.36
96 T	3.41	7.34×10^{-3}	2.74	−22.3	
Acetic acid					
6 T	4.03	9.51×10^{-3}	2.62	−35.2	
36 T	4.06	9.66×10^{-3}	2.63	−35.7	−0.610
96 T	4.07	9.68×10^{-3}	2.63	−37.5	

The NBO charge in the gas phase for the oxygen atom that interacts with Ba in the adsorbed state is also reported.

charge may serve as a simple metric for predicting the strength of adsorption of related adsorbates on BaNaY zeolites.

4. Conclusion

Before trying to model the catalytic properties of BaNaY zeolites, various combinations of ECP basis sets for barium and all-electron basis sets for non-barium atoms using the B3LYP and PW91PW91 functionals were evaluated based on predictions of the apex angle of barium dihalides and heats of reaction for barium-containing reactions in the gas phase. It was shown that the SDD basis set for barium and the D95 basis set for other atoms using B3LYP is a suitable choice for the cluster calculations for BaNaY zeolites. With this choice of basis set and level of theory, three different sizes of clusters, 6 T (pure DFT), 36 T, and 96 T (ONIOM), were utilized in order to test the convergence of the effect of the zeolitic framework on the adsorption of acetaldehyde, acetic acid, nitromethane, and water. Structures, vibrational frequencies, and adsorption enthalpies of these adsorbates were calculated. It was shown that inclusion of van der Waals interactions increased the magnitude of the adsorption enthalpy non-linearly toward an asymptotic value through the MM part, while the configurations and vibrational frequencies of the adsorbates did not change markedly. For adsorbed acetaldehyde, nitromethane, and acetic acid, NBO analysis showed that the strength of the interaction between Ba and adsorbate oxygen is reflected in four properties: the distance between Ba and the oxygen, the adsorption enthalpy, the charge transfer, and the energetic stabilization due to donor–acceptor interactions. The trends of these four properties correlate with the charge on the oxygen atom in the gas-phase molecule.

From the calculated geometries of adsorbed acetaldehyde, nitromethane, and acetic acid and the NBO analysis, it can be inferred that other stable intermediates would probably have similar configurations, i.e., an adsorbate oxygen coordinated to Ba and an adsorbate hydrogen coordinated to a framework oxygen next to an aluminum atom. These structures may help in developing a better understanding of the role that barium plays in deNO*x* catalysis in BaY zeolites. Although a very detailed mechanism has been proposed in the literature, the mechanism focuses on the reacting molecules; the roles of barium and the confining environment of the zeolite are still largely unknown.

Acknowledgments

This work was supported by the Chemical Sciences, Geosciences, and Biosciences Division, Office of Basic Energy Sciences, Office of Science, U.S. Department of Energy Grant No. DE-FG02-03ER15457. This research used resources of the National Energy Research Scientific Computing Center, which is supported by the Office of Science of the U.S. Department of Energy under Contract No. DE-AC02-05CH11231.

References

[1] N. de Nevers, Air Pollution Control Engineering, MacGraw-Hill, Boston, 2000.
[2] D. Gerard, L.B. Lave, Technol. Forecast. Soc. 72 (2005) 761–778.
[3] J.N. Armor, Catal. Today 26 (1995) 147–158.
[4] M.D. Amiridis, T.J. Zhang, R.J. Farrauto, Appl. Catal. B 10 (1996) 203–227.
[5] A.P. Walker, Catal. Today 26 (1995) 107–128.
[6] M.C. Campa, D. Pietrogiacomi, S. Tuti, G. Ferraris, V. Indovina, Appl. Catal. B 18 (1998) 151–162.
[7] B.J. Adelman, W.M.H. Sachtler, Appl. Catal. B 14 (1997) 1–11.
[8] Y.J. Li, J.N. Armor, J. Catal. 150 (1994) 376–387.
[9] H. Mahzoul, J.F. Brilhac, P. Gilot, Appl. Catal. B 20 (1999) 47–55.
[10] J.H. Kwak, J. Szanyi, C.H.F. Peden, J. Catal. 220 (2003) 291–298.
[11] J.H. Kwak, J. Szanyi, C.H.F. Peden, Catal. Today 89 (2004) 135–141.
[12] Y.H. Yeom, B. Wen, W.M.H. Sachtler, J. Phys. Chem. B 108 (2004) 5386–5404.
[13] P.J. Hay, W.R. Wadt, J. Phys. Chem. 82 (1985) 299–310.
[14] M. Kaupp, P.V. Schleyer, H. Stoll, H. Preuss, J. Chem. Phys. 94 (1991) 1360–1366.
[15] F. Maseras, K. Morokuma, J. Comput. Chem. 16 (1995) 1170–1179.
[16] L.A. Clark, M. Sierka, J. Sauer, J. Am. Chem. Soc. 125 (2003) 2136–2141.
[17] A.M. Vos, X. Rozanska, R.A. Schoonheydt, R.A. van Santen, F. Hutschka, J. Hafner, J. Am. Chem. Soc. 123 (2001) 2799–2809.
[18] X. Rozanska, R.A. van Santen, F. Hutschka, J. Hafner, J. Am. Chem. Soc. 123 (2001) 7655–7667.
[19] K. Burke, J.P. Perdew, Y. Wang, Electronic Density Functional Theory: Recent Progress and New Directions, Plenum Press, New York, 1998.
[20] A.D. Becke, J. Chem. Phys. 98 (1993) 5648–5652.
[21] M.J. Frisch, G.W. Trucks, H.B. Schlegel, G.E. Scuseria, M.A. Robb, J.R. Cheeseman, J.A. Montgomery, T. Vreven, K.N. Kudin, J.C. Burant, J.M. Millam, S.S. Iyengar, J. Tomasi, V. Barone, B. Mennucci, M. Cossi, G. Scalmani, N. Rega, G.A. Petersson, H. Nakatsuji, M. Hada, M. Ehara, K. Toyota, R. Fukuda, J. Hasegawa, M. Ishida, T. Nakajima, Y. Honda, O. Kitao, H. Nakai, M. Klene, X. Li, J.E. Knox, H.P. Hratchian, J.B. Cross, V. Bakken, C. Adamo, J. Jaramillo, R. Gomperts, R.E. Stratmann, O. Yazyev, A.J. Austin, R. Cammi, C. Pomelli, J.W. Ochterski, P.Y. Ayala, K. Morokuma, G.A. Voth, P. Salvador, J.J. Dannenberg, V.G. Zakrzewski, S. Dapprich, A.D. Daniels, M.C. Strain, O. Farkas, D.K. Malick, A.D. Rabuck, K. Raghavachari, J.B. Foresman, J.V. Ortiz, Q. Cui, A.G. Baboul, S. Clifford, J. Cioslowski, B.B. Stefanov, G. Liu, A. Liashenko, P. Piskorz, I. Komaromi, R.L. Martin, D.J. Fox, T. Keith, M.A. Al-Laham, C.Y. Peng, A. Nanayakkara, M. Challacombe, P.M.W. Gill, B. Johnson, W. Chen, M.W. Wong, C. Gonzalez, J.A. Pople Jr., Gaussian 03, Revision D. 02, Gaussian, Inc., Wallingford, CT, 2004.
[22] Y.H. Yeom, S.B. Jang, Y. Kim, S.H. Song, K. Seff, J. Phys. Chem. B 101 (1997) 6914–6920.
[23] G. Martra, R. Ocule, L. Marchese, G. Centi, S. Coluccia, Catal. Today 73 (2002) 83–93.
[24] J.A. Hriljac, M.M. Eddy, A.K. Cheetham, J.A. Donohue, G.J. Ray, J. Solid State Chem. 106 (1993) 66–72.
[25] S.A. McMillan, L.J. Broadbelt, R.Q. Snurr, J. Phys. Chem. B 106 (2002) 10864–10872.
[26] S.A. McMillan, L.J. Broadbelt, R.Q. Snurr, J. Phys. Chem. B 107 (2003) 13329–13335.
[27] S.A. McMillan, L.J. Broadbelt, R.Q. Snurr, Environmental Catalysis, Taylor and Francis, New York, 2005, pp. 287–306.
[28] K.K. Bobuatong, J. Limtrakul, Appl. Catal. A 253 (2003) 49–64.
[29] Y.V. Joshi, K.T. Thomson, J. Catal. 230 (2005) 440–463.
[30] A.K. Rappe, C.J. Casewit, K.S. Colwell, W.A. Goddard, W.M. Skiff, J. Am. Chem. Soc. 114 (1992) 10024–10035.
[31] S.A. McMillan, Modeling nitrogen oxide catalysis over cobalt-exchanged zeolites: the role of cobalt-zeolite coordination environment, Ph.D. Thesis, Northwestern University, 2003.
[32] F.B. Vanduijneveldt, J.G.C.M.Vanduijneveldtvande. Rijdt, J.H. Lenthe, Chem. Rev. 94 (1994) 1873–1885.
[33] A.E. Reed, L.A. Curtiss, F. Weinhold, Chem. Rev. 88 (1998) 899–926.
[34] F. Weinhold, C.R. Landis, Valency and Bonding: A Natural Bond Orbital Donor–Acceptor Perspective, Cambridge University Press, New York, 2005.
[35] V. Calder, D.E. Mann, K.S. Seshadri, M. Allavena, D. White, J. Chem. Phys. 51 (1969) 2093–2099.

[36] D. White, G.V. Calder, S. Hemple, D.E. Mann, J. Chem. Phys. 59 (1973) 6645–6651.
[37] J.W. Hastie, R.H. Hauge, J.L. Margrave, High Temp. Sci. 3 (1971) 56–72.
[38] M. Hargittai, M. Kolonits, G. Schultz, J. Phys. Chem. A 567 (2001) 241–246.
[39] M.W. Chase, NIST-JANAF Themochemical Tables, fourth ed. J. Phys. Chem. Ref. Data, Monograph 9 1998, 1-1951.
[40] J.C. Moise, J.P. Bellat, A. Methivier, Microporous Mesoporous Mater. 43 (2001) 91–101.
[41] C. Xu, B.E. Koel, J. Chem. Phys. 102 (1995) 8158–8166.
[42] J.B. Levy, M. Hargittai, J. Phys. Chem. A 104 (2000) 1950–1958.
[43] M. Kaupp, P.V. Schleyer, H. Stoll, H. Preuss, J. Am. Chem. Soc. 113 (1991) 6012–6020.
[44] C. Angeli, S. Borini, L. Ferrighi, R. Cimiraglia, J. Mol. Struct. (Theochem.) 718 (2005) 55–69.
[45] I.V. Tokmakov, V.A. Shlyapochnikov, J. Mol. Struct. (Theochem.) 46 (1997) 1992–1995.
[46] A. Burneau, F. Génin, F. Quilès, J. Mol. Struct. (Theochem.) 2 (2000) 5020–5029.